J Nondestruct Eval (2008) 27: 35–45
DOI 10.1007/s10921-008-0035-3

Characterization of Reflector Types by Phase-Sensitive Ultrasonic Data Processing and Imaging

Klaus Mayer · Karl-Jörg Langenberg · Martin Krause · Boris Milmann · Frank Mielentz

Published online: 1 July 2008

Abstract Ultrasonic and radar imaging techniques are limited in resolution by the wavelength in the material, yet information beyond those limits is hidden in complex frequency dependent reflection coefficients. The analysis of the phase of complex reflection coefficients together with the properties of imaging algorithms can help to characterize and to classify indications of defects in concrete buildings. This paper describes a method to extract phase information from measurements and SAFT reconstructed images. The influencing factors like material properties, transducer characteristics, and imaging algorithms based on Born or Physical Optics approximations are elaborated. Simulated and experimental results are briefly discussed.

Keywords NDT · Imaging · Flaw characterization · Tendon ducts · Phase analysis · Ultrasonic echo · SAFT · FT-SAFT · EFIT-modeling

1 Introduction

Recent studies demonstrated the possibility of using imaging algorithms like SAFT (Synthetic Aperture Focusing Technique) [1, 2] or FT-SAFT (Fourier Technique SAFT) [3, 4] for non-destructive testing (NDT) of concrete with ultrasound and radar. Adapted to the grain size of the aggregates, ultrasonic measurements at frequencies between 50 and 200 kHz have been performed. In particular the introduction of point contact transducers allows for scanning of large areas of concrete structures to answer specific questions about the condition of reinforcement and tendon ducts. One goal is to examine the interior of tendon ducts to detect grouting defects which remove the natural conservation of steel in concrete or mortar against corrosion and may in the long term lead to degradation of the building stability. As SAFT was used initially for NDT of steel components there was no need examining the signal in detail because voids and cracks, which should be distinguished, do have reflection coefficients of the same sign and the signals are rectified or envelope detected anyway [5]. The problem of assessing the integrity of tendon ducts in concrete and the use of broadband transducers requires and allows a more detailed approach.

In concrete the wave propagation is distorted by the stochastic arrangement of aggregates with different acoustic properties and air voids. The methods which are based on the analysis of time delay require that the wave fronts stay together and this is only the case if the wavelength is larger than the aggregates. This fact leads to a resolution limitation of the imaging algorithm, being in the range of the wavelength. In concrete with a typical average shear wave speed of $c_s = 2600$ m/s the wavelength at a frequency of 55 kHz is 47 mm. It is evident that objects like tendon ducts can be detected but the content cannot be accurately imaged. A solution is offered by combining this method with a phase analysis of the reconstructed image [6].

Being based on certain approximations imaging algorithms like SAFT calculate a "band limited" object function of the scattering object. "Band limited", however, means that the reconstruction is resolution limited and oscillating. These oscillations are a source of irritation and unique peak

K. Mayer (✉) · K.-J. Langenberg
University of Kassel, 34109 Kassel, Germany
e-mail: kmayer@uni-kassel.de

M. Krause · B. Milmann · F. Mielentz
Federal Institute for Materials Research and Testing (BAM), 12200 Berlin, Germany

detection would not be possible—at least not by visual inspection of the images. This is the reason why during conventional SAFT processing an envelope is calculated which suppresses the oscillations. In this step the phase information is lost, too. A second problem is based on the fact that SAFT-like methods are mathematically derived under an assumption which is not fulfilled in the actual application: SAFT does not take into account multiple reflections, i.e., parts of the signal which are caused by multiple reflections are not focused to those positions where they occur physically but lead to artifacts—ghost images—degrading the expected image. Those artifacts are recognizable if the multiple reflections are separated in the time range. But this is not the case if the multiple echoes superimpose and combine to one single indication. In addition to that, a real life measurement does not fulfill the ideal conditions which were assumed for the development of the imaging algorithms [4]. The artifacts in the imaging results are known but the influence on the phase analysis is widely undocumented. The most important influencing factors are: the spatial property of a wave field transmitted and received by a real antenna or transducer, the finite extent of the measured surface (aperture) which in combination with a finite beam angle of the transducer leads to effects dependent on the position of the scattering event, and the dispersive and dissipative property of material with a strong heterogeneous structure like concrete. These influences will be analyzed in the next sections in addition to the explanation of the phase analysis itself and a multidimensional version which accounts for the influence of the finite aperture of real measurements.

2 Imaging Algorithms

The propagation of mechanical waves is induced by elastic deformations of a body due to forces being applied on the surface of the body. These waves propagate as pressure and shear waves with different velocities converting into each other at boundaries by mode conversion. Elastic waves are generated and detected by piezoelectric converters which allow the detection of wave field components. From such components the different wave types may be gained by time gating or by more sophisticated vector processing [4, 5]. To get the full information out of a measurement it is usually not enough to do a scalar processing. But as all algorithms are based on linearizing assumptions, their influence on the phase detection scheme is comparable for scalar as well as for elastic and electromagnetic waves.

Starting point for imaging algorithms like SAFT is a scalar wave equation, e.g. an acoustic wave describing the spatial and temporal propagation of the pressure $p(\underline{\mathbf{R}}, t)$ ($\underline{\mathbf{R}}$ is the position vector to the observation point in space, t is the time, and ∇ is the del-operator), whereby the sources may occur as force density $\underline{\mathbf{f}}(\underline{\mathbf{R}}, t)$ or dilatation rate $h(\underline{\mathbf{R}}, t)$:

$$\nabla \cdot \nabla p(\underline{\mathbf{R}}, t) - \rho(\underline{\mathbf{R}})\kappa(\underline{\mathbf{R}}) \frac{\partial^2 p(\underline{\mathbf{R}}, t)}{\partial t^2} = \nabla \cdot \underline{\mathbf{f}}(\underline{\mathbf{R}}, t) + \rho(\underline{\mathbf{R}}) \frac{\partial h(\underline{\mathbf{R}}, t)}{\partial t}. \tag{1}$$

The material properties are hidden in the mass density $\rho(\underline{\mathbf{R}})$ and the compressibility $\kappa(\underline{\mathbf{R}})$. Let us consider a material (of infinite extent) supporting acoustic waves having a constant mass density ρ and a constant compressibility κ; a scattering object of finite volume V_c with surface S_c is embedded in this material whose geometry is given by the characteristic function $\Gamma_c(\underline{\mathbf{R}})$ of V_c:

$$\Gamma_c(\underline{\mathbf{R}}) = \begin{cases} 0 & \text{for } \underline{\mathbf{R}} \notin V_c, \\ 1 & \text{for } \underline{\mathbf{R}} \in V_c. \end{cases} \tag{2}$$

We assume that the mass density inside V_c is the same as outside, yet we admit an inhomogeneous compressibility $\kappa(\underline{\mathbf{R}})$ inside V_c. This scattering object is illuminated by an incident field coming from a finite source volume V_Q supporting only a non-zero dilatation rate $h(\underline{\mathbf{R}}, t)$, i.e., we do not allow for a force density $\underline{\mathbf{f}}(\underline{\mathbf{R}}, t)$. In order to identify an inverse problem we need data: these should be the pressure $p(\underline{\mathbf{R}}, t)$ on a (fictitious) surface S_M enclosing the volume V_M. The NDT problem as an inverse scattering problem is then posed as follows: with the knowledge of the incident field and $p(\underline{\mathbf{R}}, t)$ on S_M find the location of V_c and $\kappa(\underline{\mathbf{R}})$ within V_M. With the definition of the compressibility contrast

$$\chi_\kappa(\underline{\mathbf{R}}) = \frac{1}{\kappa}\big[\kappa(\underline{\mathbf{R}}) - \kappa\big]\Gamma_c(\underline{\mathbf{R}}) \tag{3}$$

an inhomogeneous compressibility is defined as:

$$\kappa(\underline{\mathbf{R}}) := \kappa\big[1 + \chi_\kappa(\underline{\mathbf{R}})\big] = \begin{cases} \kappa & \text{for } \underline{\mathbf{R}} \notin V_c, \\ \kappa(\underline{\mathbf{R}}) & \text{for } \underline{\mathbf{R}} \in V_c \end{cases} \tag{4}$$

for *all* points in space inside and outside V_c.

Following the derivation in [4] one ends up with a solution for the inverse problem under the limitation of the Born approximation in the frequency domain with the wave number $k = \omega/c$, defined by the frequency ω and the wave velocity $c = 1/\sqrt{\kappa\rho}$. This solution is based on the representation of the scattered pressure p_s^{Born} in terms of a superposition of linearized secondary sources involving the frequency domain free-space Green's function $G(\underline{\mathbf{R}} - \underline{\mathbf{R}}', \omega)$:

$$p_s^{\text{Born}}(\underline{\mathbf{R}}, \omega) = k^2 \iiint_{V_c} \chi_\kappa(\underline{\mathbf{R}}')\, p_i(\underline{\mathbf{R}}', \omega) G(\underline{\mathbf{R}} - \underline{\mathbf{R}}', \omega)\, \mathrm{d}^3\underline{\mathbf{R}}'. \tag{5}$$

This indeed is a linearization: the unknown total field in the secondary sources is replaced by the known incident field $p_i(\underline{\mathbf{R}}', \omega)$ and, therefore, a solution for the unknown scattering object $\chi_\kappa(\underline{\mathbf{R}})$ can be easily derived for many measurement setups through inversion of the integral (5). A prominent solution is given by the Fourier Diffraction Slice Theorem for plane wave incidence yielding the Fourier Domain SAFT algorithm which, by some minor modifications, leads to the bistatic or pitch-catch time domain SAFT algorithm [3].

Considering the very common experimental setup in NDT—the impulse echo method or the monostatic case—where the transmitting and receiving transducers/antennas are moved synchronously separated by a very small distance or coinciding physically—the excitation has to be chosen as a point source yielding the monostatic version $p_s^{\mathrm{Born,m}}(\underline{\mathbf{R}}, \omega)$ of (5). Yet, before the data can be utilized for inversion, some filtering has to be performed. The modified monostatic data $p_s^{\mathrm{Born,mo}}(\underline{\mathbf{R}}, \omega)$ must be calculated according to

$$p_s^{\mathrm{Born,mo}}(\underline{\mathbf{R}}, \omega) = \frac{2\pi}{\mathrm{j}} \frac{\partial}{\partial k} \frac{p_s^{\mathrm{Born,m}}(\underline{\mathbf{R}}, \omega)}{k^2 p_0(\omega)}, \tag{6}$$

where $p_0(\omega)$ is the frequency spectrum of the incident pulse, and j denotes the imaginary unit. Defining the three-dimensional spatial Fourier transform of the contrast according to

$$\tilde{\chi}_\kappa(K_x, K_y, K_z) = \int_{-\infty}^{\infty}\int_{-\infty}^{\infty}\int_{-\infty}^{\infty} \chi_\kappa(x, y, z)\mathrm{e}^{-\mathrm{j}K_x x - \mathrm{j}K_y y - \mathrm{j}K_x z}\mathrm{d}x\mathrm{d}y\mathrm{d}z \tag{7}$$

as well as the two-dimensional Fourier transform of the modified scattered pressure with regard of the measurement plane coordinates x, y ($z = d$ is the distance from the origin) we obtain:

$$\tilde{\chi}_\kappa(K_x, K_y, K_z) = -2\mathrm{j}K_z\mathrm{e}^{-\mathrm{j}dK_z}\hat{p}_s^{\mathrm{Born,mo}}(K_x, K_y, d, \omega) \tag{8}$$

$$\text{with } K_z = \sqrt{4k^2 - K_x^2 - K_y^2} \geq 0 \tag{9}$$

as inversion of (5) after modification.

Obviously, (8) is a linear relation between the scattered field $\hat{p}_s^{\mathrm{Born,mo}}(K_x, K_y, d, \omega)$ in the respective Fourier space and the Fourier transformed contrast function.

3 Phase Analysis

The above brief mathematical derivation of the imaging algorithm exhibits the underlying linearization, i.e., multiple scattering manifesting as resonances or as complex reflection coefficients for object sizes in the range of the wavelength. Multiple scattering data do not enter into the explicit geometry calculation; instead, they blur the geometry or render it as complex-valued. As a consequence, additional information about the scattering process beyond the resolution limit, as given by the bandwidth of the signal, may be extracted either in the time domain, i.e., from the data itself, or from the image (contrast reconstruction) e.g. by phase analysis of the complex reflection coefficients.

In general, the analysis of the reconstructed image is preferred, as the scattering centers are separated in space whereas in the B-scans (space/time data) the signals of different scattering centers interfere. It should be kept in mind that the reconstruction is phase invariant only if the other assumptions, e.g. constant background velocity, are fulfilled. If this is not the case the analysis of the data itself is favorable.

For the example of the reflection of an ultrasonic elastic shear wave from a steel plate embedded in concrete the transition from separable multiple scattering to overlapping impulses is observable for decreasing thickness of the plate. In Fig. 1 the thickness of the plate varies from 0 to 100 mm under an incident raised cosine (RC2) signal with the centre frequency of 55 kHz corresponding to a wavelength of 47 mm in the background medium with $c_s = 2600$ m/s. Mode conversion does not occur for perpendicular incidence as chosen here. The deformation of the signal is remarkable if the multiple reflections coincide. The symmetric RC2 signal changes into a nearly antisymmetric signal manifesting itself in a complex frequency dependent reflection coefficient.

As seen in Fig. 1b, the analysis of scattered signals is not trivial. The scattered time domain signal of a plate is the total wave train consisting of an infinite number of multiple reflections. The complex value of the frequency domain reflection coefficient of a layer, which can be calculated analytically, contains all those multiple reflections. In case of separated impulses, only the first one is significant in practice. The remaining parts will appear as artifacts in the reconstruction. If the impulse train is compressed, only one scattering centre will appear but it will be displaced and broadened. In that case, phase detection is necessary to extract some more hidden information.

As the position and the geometry of the scatterer are unknown quantities reproducible delay estimation, respectively location estimation, must precede the phase estimation. To achieve this, the envelope of the analytic signal of the impulse is used because this quantity has to be computed anyway within the imaging algorithms via the Fourier space. In time domain SAFT processing, this envelope is used to suppress the oscillations of the band limited signals which otherwise would show up in the image.

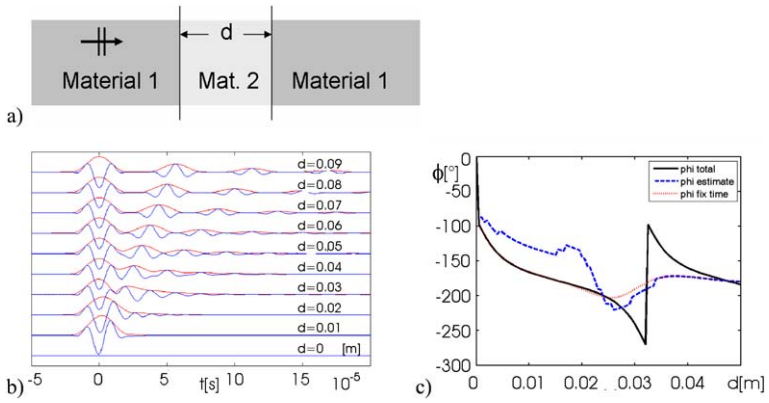

Fig. 1 Simple model to demonstrate the phase estimation: **a** Geometry of 2 materials, concrete/steel/concrete. **b** Reflected RC2 signal with $f_0 = 55$ kHz, with mathematical envelope. **c** Comparison of phases ϕ with variation of the thickness of the steel plate; *solid line*: exact phase of the multiple scattering event, *blue dashed line*: estimated phase with the maximum of the envelope as reference, *red dotted line*: phase estimated with a fixed reference time ($t_0 = 0$ s)

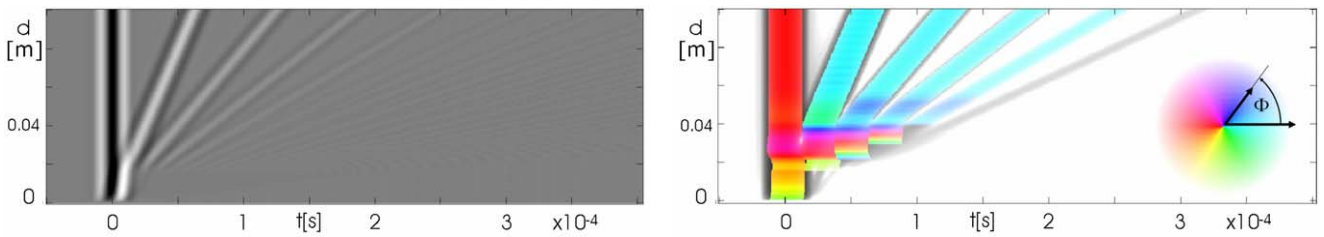

Fig. 2 Three-Layer-Model: **a** Collection of A-scans if the thickness d of the plate is varying continuously. **b** Visualization of the estimated phase in the A-scans by a mixed color table (see text). This color table—displayed as a color wheel—is used for most of the following images

3.1 Estimation of the Phase

We should distinguish between the calculation of the phase of the data and the phase of a scattering event in the reconstructed image. As phase of an impulse in the data the phase of the spectral component f_0 within the interval $[t_0 - 1/f_0, t_0 + 1/f_0]$ is used. Preferably, the frequency f_0 is the centre frequency of the transducer, and t_0 is the maximum of the envelope of the impulse calculated by the magnitude of the analytic signal. In the reconstructed image the phase of a scattering indication at a depth z_0 is defined as the phase of the spectral component at the wavelength in the image λ_i within the interval $[z_0 - \lambda_i, z_0 + \lambda_i]$. Only those values of the images which exceed a certain threshold value are used for interpretation.

In [7] we describe the influence of the phase detection for a plate with variable thickness. As mentioned there the position of the maximum changes in relation to changes in the thickness of the plate, because the envelope is an integral quantity, whereas the reference point of the exact phase—determined analytically—remains unchanged at the front of the plate. Therefore, the exact value of the phase cannot coincide with the value derived from the impulse by the scheme above. Figure 1c compares the results for the calculations at the centre frequency. The difference is clearly visible and also that critical value, if the thickness of the plate is large enough, so that the estimation scheme is able to separate the pulses. If the thickness of the plate reaches that critical value the observed phase jumps to the phase of the incident pulse, which is 0° or 180° depending on the material properties.

3.2 Visualization of Results

In the field of ultrasonic NDT the graphical display of scattered data and reconstructed images is done by grey or color scaled intensity images with a non standardized color table as seen in Fig. 2a. For the display of the phase a combination of a grey and a color table is appropriate: those parts of the signal below a certain threshold value are displayed in a grey scale and the phase of detected pulses is coded according to an appropriate color table (Fig. 2b). The intensity of the original signal may be visualized additionally as the color saturation of the indication.

4 Influencing Factors

In the following, we deal with different factors affecting the accuracy of the determination of the exact phase of the scattering process. These factors include the transmitting and

receiving transducers/antennas, the possibly dispersive material, and the imaging algorithms.

4.1 Transmitting/Receiving Transducers

The ultrasonic data acquisition on concrete is performed with piezoelectric transducers, whereas radar uses aperture antennas. Besides their electrical properties whose influence may be eliminated by appropriate deconvolution methods both signal converters exhibit a finite aperture which results in an integration effect related to the aperture size. This integration leads to a non-uniform spatial phase characteristic and is specific for any transducer or antenna type, respectively. In the following, we investigate the radiation properties of a point contact transducer used for the excitation of elastic shear waves by means of the 3D Elastodynamic Finite Integration Technique (3D EFIT simulation) [8, 9]. The transducer consists of a rectangular array of 3×4 transmitters and the same number of receiver devices whose signals are superimposed. Figure 3 shows the propagation of elastic waves from a single element as compared to the two-dimensional arrangement of the 3×4 elements. With such simulations the time dependent behavior and, hence, the phase property can be calculated at each point in space. Here the signal and phase behavior along the symmetry axis between transmitter and receiver are shown.

A typical effect in the near-field is that those parts of the wave field coming from the edges of the excitation aperture reach the observation point later than the wave field from the centre of the aperture. This delay leads to an impulse deformation and therefore to an overall phase shift as displayed in Fig. 3. The fact that the received signal is a convolution of the exciting signal with the impulse responses of the scattering process as well as with the receiver device leads to the superposition of the individual phase properties in the frequency domain. Therefore the influence of the incident field can be eliminated by separate measurements for calibration or by analytical or numerical computation of the incident field properties.

4.2 Influence of the Propagation Material

Within homogeneous isotropic non-dispersive and non-dissipative materials there is no signal distortion and therefore no influence on the observed phase. Within strong heterogeneous materials like concrete this is not expected. Due to scattering the wave front loses energy, and this loss depends on the relation of the wavelength to the size of the scatterers and, therefore, it is frequency dependent.

Theoretical considerations, measurements, and numerical simulations show that higher frequencies are more attenuated than lower frequencies and that the centre frequency of the received signal decreases if the propagated distance of the wave increases. This is a statistic process which, on the average, leads only to a small signal deformation and can therefore be neglected when compared to the statistic fluctuations of single measurements.

A much stronger influence has the coda, i.e., that part of the signal, which is due to multiple scattering. It can only be minimized by increasing the size of the transducer. This implies an averaging operation suppressing the non-coherent part of the coda. Fortunately, the averaging properties of imaging algorithms like SAFT yield the same effect. The coherent superposition of signals from different positions, each having a different coda, lead to a restoration of the wave front.

Figure 4 shows the estimated phase variation along the depth coordinate beneath a 56 mm transducer. The material is modeled by 4 different aggregates in a cement mortar matrix with largest grain size of 16 mm and a porosity content of 1%. Figures 4c and d compare the phase detection obtained with two receiver models: a point like receiver and a receiver aperture of 56 mm. It is clearly visible that, in the first case, the influence of the coda disturbs the wave front signal, whereas the averaging virtual transducer restores the signal, leading to a proper determination of the signal phase, even in the presence of loss of bandwidth. Of course, such a virtual transducer can only be realized via simulation, but it helps to understand the basic effects.

4.3 Influence of the Imaging Algorithm

As mentioned above, for heterogeneous media it is more reasonable to determine the phase from the reconstruction as it is less sensitive to multiple scattering interferences. Nevertheless, some remarks are necessary: Imaging algorithms like SAFT are based on the principle of coherent superposition being derived from diffraction theory. However, the derivation implies approximations which have to be taken into account when interpreting the results. In addition, in most cases only a one sided measurement is available, which, together with the aforementioned approximations results in *complex* reflection coefficients.

4.3.1 Phase Estimation along z-lines

If the measurement surface encloses a small scatterer the phase indication from different sides would be different in sign, so that they compensate each other in a SAFT image from all data. Regarding a single-sided access to the scatterer, it is in most cases sufficient to analyze the reconstruction in depth (z-) direction with the described method (Fig. 5). The centre frequency has to be replaced by $1/\lambda_i$ (λ_i denotes the wavelength in the SAFT-image which is, due to the monostatic set-up, 0.5 times the wavelength in the material).

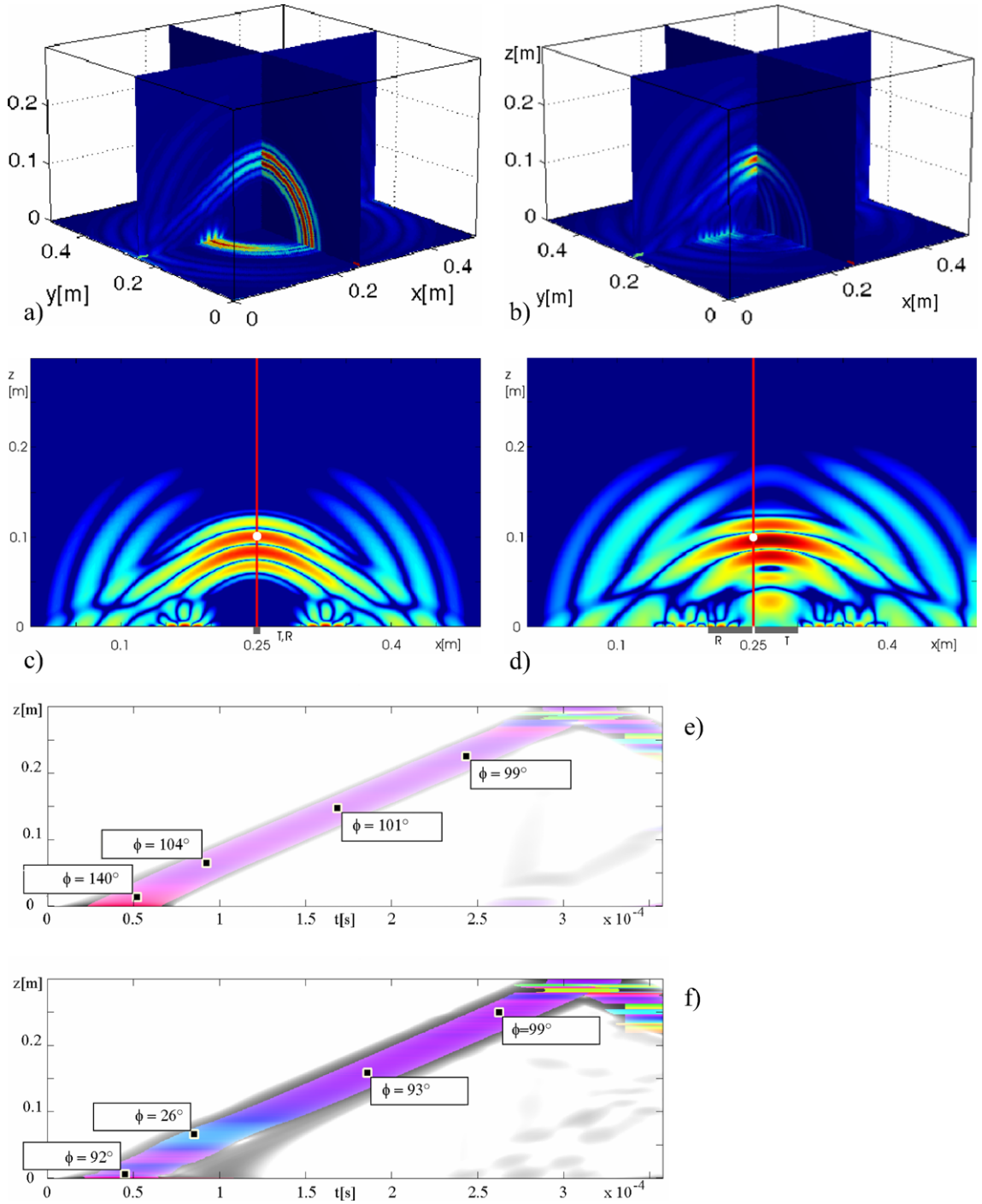

Fig. 3 Phase estimation for point contact transducers simulated with EFIT. *Left*: One single point contact element. *Right*: Arrangement of a 3×4 array of point contact elements as transmitters right to the origin. **a**, **b** Magnitude of the particle velocity $\underline{\mathbf{v}}$. Slices along the axis of a $0.5 \times 0.5 \times 0.3$ m^3 cuboid, excitation: 55 kHz RC2, shear in x-direction. **c**, **d** Magnitude of a x, z-slice of the x-component (logarithmic scale) of $\underline{\mathbf{v}}$. **e**, **f** Estimated phase along the centre line displayed in z, t-coordinates to identify the transition between near and intermediate range of the transducer (color map: see Fig. 2b)

4.3.2 Multidimensional Phase Estimation

The above one-dimensional approach is not totally correct because a scatterer whose image is obliquely oriented would be obliquely crossed by the phase identification algorithm resulting in a larger wavelength in z-direction, i.e., the phase analysis would take place at the wrong frequency. Fortunately, numerous experiments show that the proposed

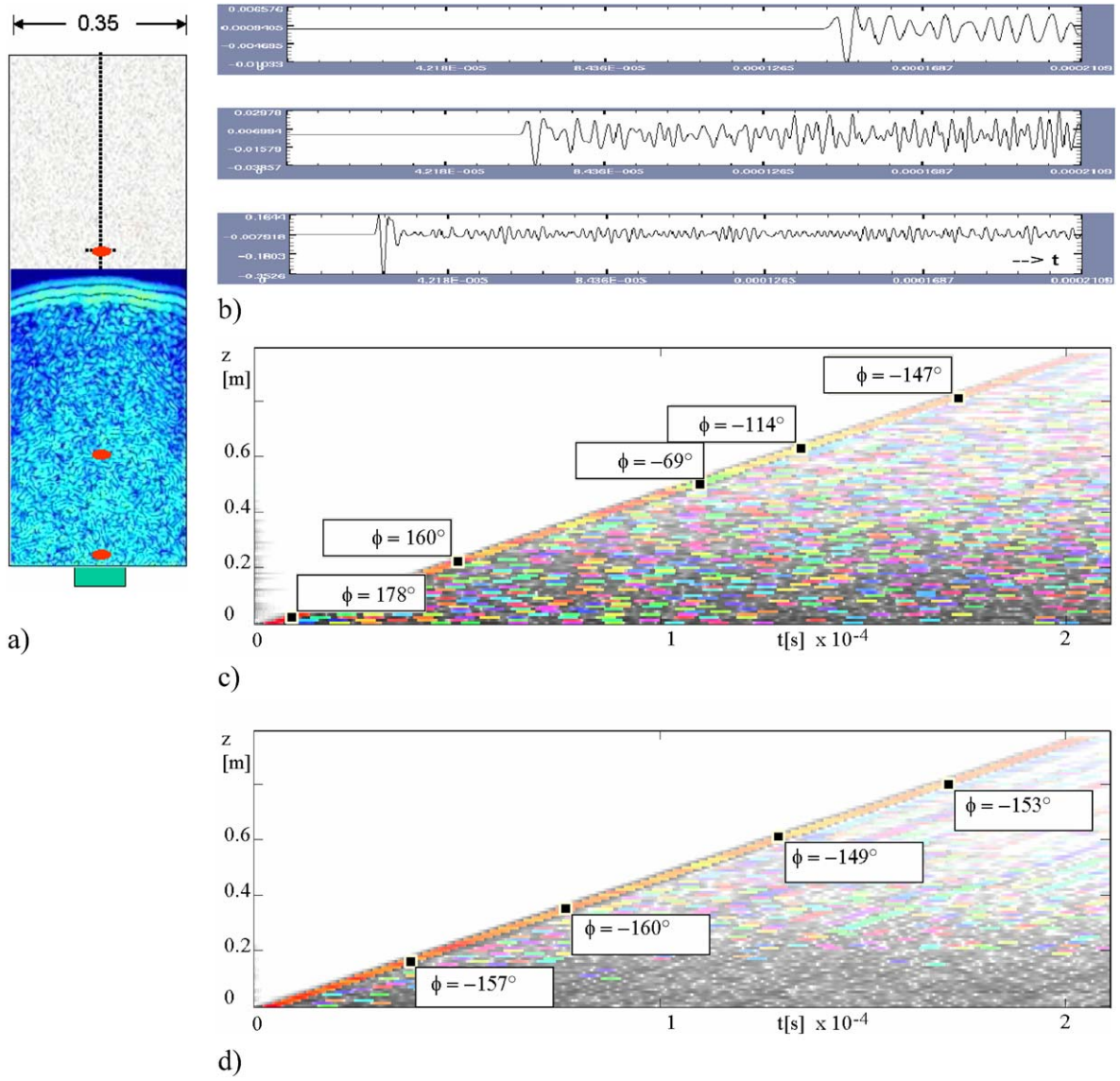

Fig. 4 Wave propagation in concrete: **a** Concrete material with 16 mm aggregates and 1% air inclusion. Geometry and snapshot of a pressure wave excited with RC2 signal, 400 kHz, modeled with EFIT-2D. **b** Signals on the centre line of the transducer at 0.1 m, 0.3 m, and 0.7 m (*red dots*). Size of the block: 1 m × 0.35 m. The centre frequency decreases to 100 kHz at 0.7 m. **c** Phase estimation of signals on the centre line: signal of a point like receiver. **d** Signal integrated by a 56 mm virtual receiver (color map: see Fig. 2b)

method for the phase analysis is not very frequency dependent. To avoid that problem totally a 2D- or a 3D-method would be necessary. One proposal is to detect the scattering centre in the same way as mentioned above by maximum value detection of the envelope in z-direction. For any detected point a 2D- or 3D-Fourier transform of a neighborhood of ± 1 wavelength around the point is performed and the maximum on a circle (a sphere in 3D) in the Fourier space with the radius of $2\pi/\lambda_i$ is searched. This complex spectral value is then used for phase determination. Therewith it is assured that the prominent scattering amplitude is used for phase determination at the correct frequency. The direction information contained in the position of the spectral value can be used additionally for the visualization of the phase. Figure 6 demonstrates this approach for an example of NDT of tendon ducts. A concrete specimen—containing a tendon duct with synthetic grouting defects (refer to specimen NB-FBS1.BAM in [1, 10])—is scanned by an ultrasonic array with 10 times 4 shear wave point contact transducers at 55 kHz. The 3D FT-SAFT image is calculated by a specialized Fourier technique and displayed together with a phase image of one x, y-slice. The influence of the finite aperture of the transducer (which is 0.3 m) is important—as discussed later—yielding an angle dependent illumination of the scattering objects. The 2D phase estimation scheme

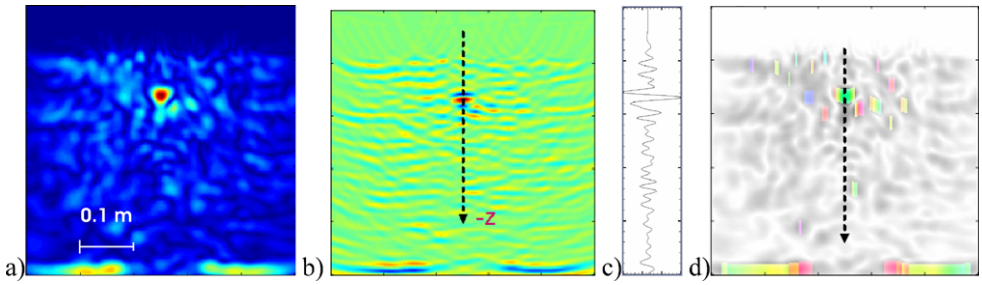

Fig. 5 Phase calculation in a one-sided measurement: Principle steps to analyze the phase of a reconstructed image. **a** Conventional FT-SAFT-image of a tendon duct with steel cables in concrete with aggregates simulated with 2D-EFIT. **b** Real part of the image. **c** 1D-plot of the reconstructed image along the dashed line. **d** Phase calculation displayed as rainbow colors in the grey scale image showing the FT-SAFT result below a predefined threshold value

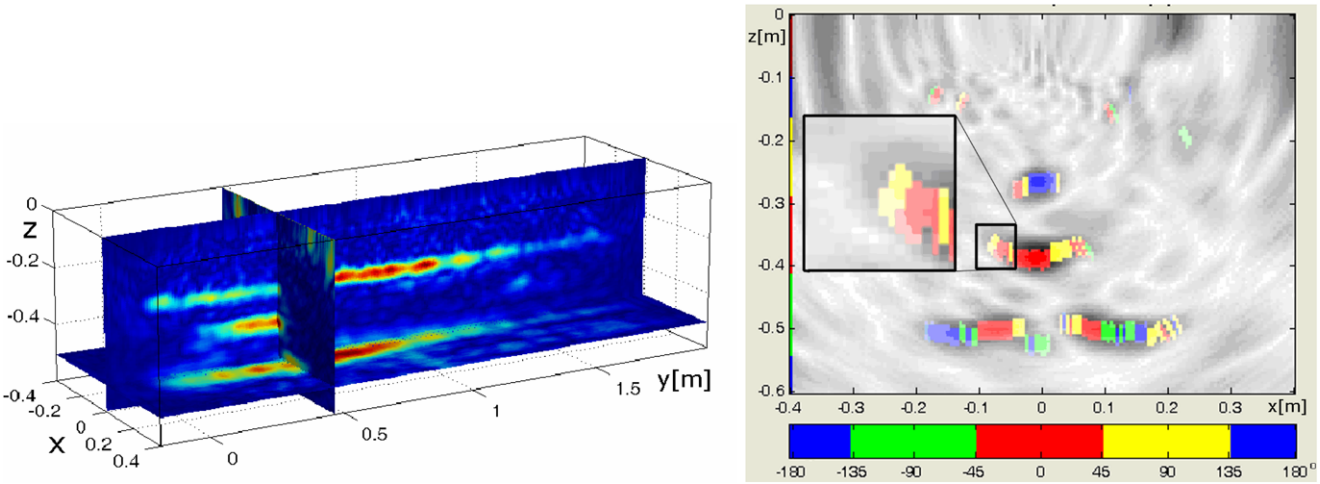

Fig. 6 Result of the 2D phase analysis. *Left*: 3D view of a 3D-FT-SAFT reconstruction of specimen NB-FBS1.BAM. Data are acquired by a 55 kHz linear array of point contact transducers. *Right*: phase displayed by 4 colors with indication of the direction of the analysis (*zoomed area*)

recognizes this dependency and the phase values as well as the direction of detection can be visualized in the image.

4.3.3 Visual Detection of the Phase

In case the depth of the scatterer is known and the shape of the excitation signal is appropriate, an alternative to the automated phase estimation method is to observe the real part of the instantaneous value of the reconstructed image. Small changes in the phase are clearly visible as changes of zero crossings of the oscillation, and may be visualized by using sign-dependent coloring. Figure 7 shows a C-scan of a 3D-SAFT image in the depth of the tendon duct and the defect is detected immediately. The measurement has been performed at the same specimen as above (NB-FBS1.BAM), but with conventional impulse echo technique. Even if the result looks very convincing, it should be taken into account, that the phase jump in the example should be about 90° and small changes of the depth of the scatterer would give similar indications, whereas an explicit phase calculation is more or less independent of the depth of the scatterer.

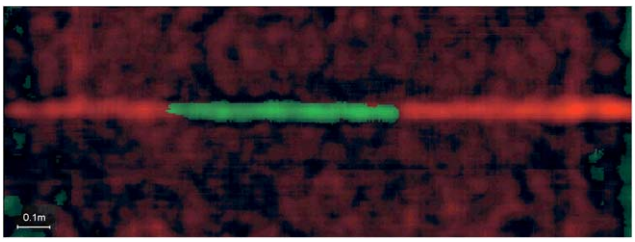

Fig. 7 Display of the real part of the C-scan (projection of some slices) of a 3D-SAFT reconstruction with sign-dependent color table

4.4 Influence of Limited Aperture

An already mentioned additional influencing factor for imaging algorithms is the limited measurement aperture. Abrupt transitions within the data at the edges of the aperture manifest themselves as artifacts in the reconstructed image; they are unphysical and therefore the phase detection will be incorrect. For smaller scattering objects the aperture limitation results in so called focus crosses (Fig. 8). Those artifacts, besides the scattering indication, will be interpreted

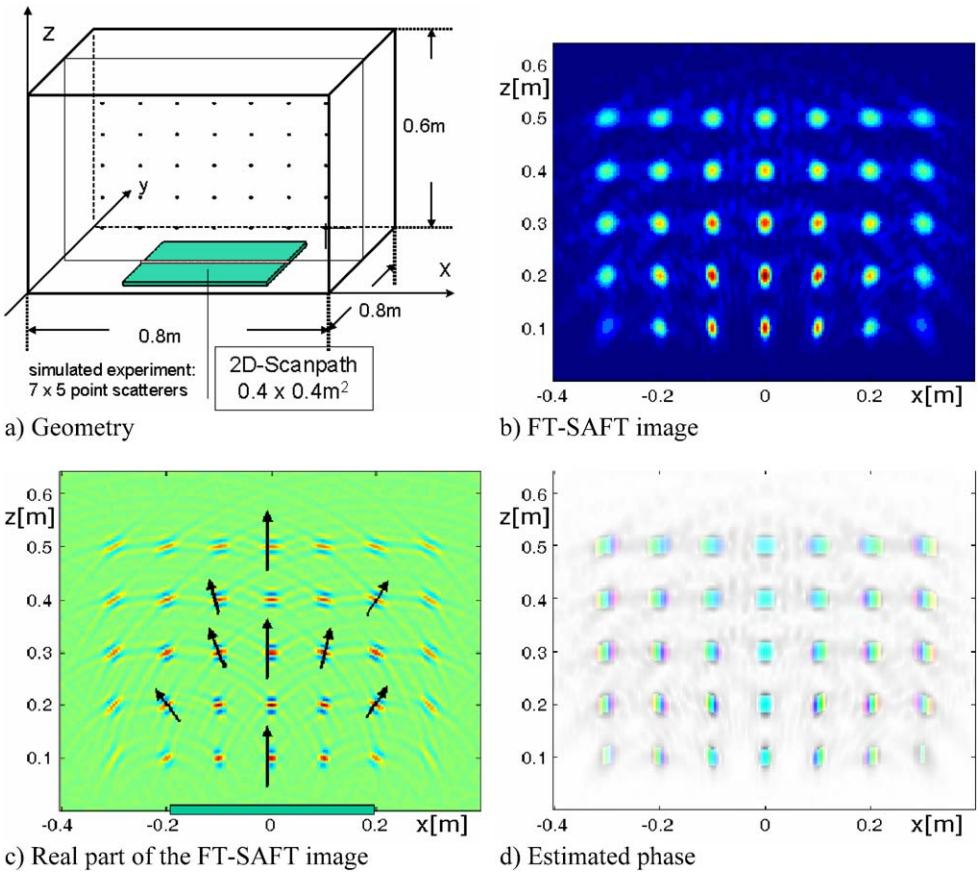

Fig. 8 Simulation to demonstrate the effect of a limited aperture. An array of 35 point like scatterers in (**a**) gives at 55 kHz a scalar impulse-echo FT-SAFT image (**b**), whose real part is displayed in (**c**) together with the phase analysis in (**d**). Because of the limited aperture, the scatterers in the regions *left* and *right* of the scanned area are slanted and the phase estimation is disturbed outside of the centre of the scatterer

incorrectly. Therefore it is recommended to use the detected phase of the midpoint of a scattering indication.

5 Application Examples

Grouting defects in tendon ducts are of central importance for NDT of prestressed concrete structures (especially bridges of reinforced concrete are concerned) because of the risk to hidden corrosion. Therefore, examples of this kind have been selected to demonstrate the capabilities of the phase sensitive evaluation.

As a real life application, the large area measurements performed on a concrete autobahn bridge in Vienna, Austria, is used [11]. The 3D-FT-SAFT reconstruction of the six layers of tendon ducts with a diameter of 40 mm, filled with a 32 mm tie rod, is depicted in Fig. 9. Prior to the measurement, it was known that the upper- and the lowermost tendon ducts (numbered for $x = 1.2$ m) were not completely grouted. This was verified by an endoscope, the corresponding bore holes lead to a high reflection magnitude at $x = 3.70$ m. In the magnitude representation of the measured area (Fig. 9a), the uppermost tendon duct shows an intense reflection compared to the other identical ducts, thus fulfilling the indication of a grouting fault, but this is not the case for the lowermost duct. The whole duct is imaged rather weakly, which might be caused by bad coupling conditions. In contrast the phase representation of the same area (Fig. 9b) indicates a phase shift of about 0° for the upper (A) and the lower duct (B), against 120° for other ducts and therefore these indications are interpreted as air reflection. This confirms the bad grouting condition predicted by applying the endoscope. It is interesting to see in this example, that the phase indication shows anomalies even if the magnitude of the reconstruction gives only very small reflection amplitudes.

A complementary technique to localize tendon ducts and other structures in concrete is the application of pulse radar [12]. Because the mathematics of electromagnetic as well as of acoustic and elastic wave propagation is closely related, similar algorithms can be used to focus the radar waves back to the scattering obstacles [5]. Therefore the discussion of the phase estimation above holds for electromagnetic waves, too. The reader is referred to [7] for an example of this application.

6 Conclusion

The observation of the phase of signals or of indications from imaging processes like SAFT or FT-SAFT gives a su-

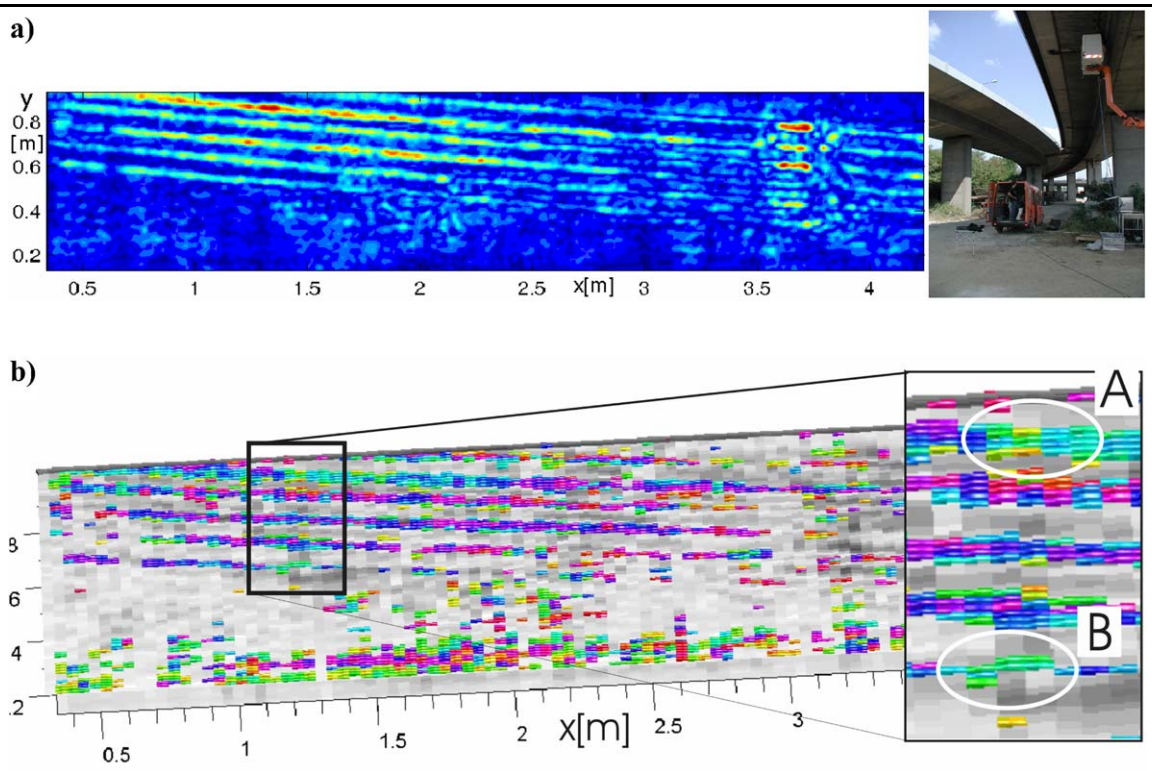

Fig. 9 Amplitude and phase image of a 3D-FT-SAFT reconstruction obtained for a bridge building. **a** C-scan image in the depth of the first layer of tendon ducts, and **b** 3D visualization of the phase indication by colored cubes. An additional black and white coded C-scan layer is displayed interactively to indicate the amplitude of scatterers and to hide indications of deeper layers of tendon ducts, which otherwise would give confusing results (color map: see Fig. 2b)

perior knowledge of the scattering process and can successfully be used for classification of many types of scattering problems in the field of NDT. The exact value of the phase depends on many variables, so it is important to observe those influences and distinguish them from real indications. Most of the influences—media, transducer, and imaging algorithm—can be taken into account by appropriate calibration measurement. The influences of the limited observation angle, sometimes combined with a limited aperture, are hard to suppress and should carefully be separated from properties of the scattering progress. Phase values not equal 0° and 180° are connected to the fine structure of the object, but they are integral values, because they occur beneath the resolution limit given by the wavelength. Therefore, these values do not describe the scattering object uniquely. But with some knowledge about the scattering object, discrimination can often be achieved easily [13]. The application to concrete is complicated because of some other effects. As recent comparisons of theoretical and experimental results show, the influence of the transition zone of concrete to steel plays an important role for phase determination. In practice, there may be such a huge amount of small air pores around the tendon duct, that the indication is irritated strongly even if the integrity of the structure is—according to standard rules—not affected [14]. Further investigation should help to clarify those problems.

Acknowledgement The support of this study by the Deutsche Forschungsgemeinschaft (German Research Foundation) via grant number FOR 384 of the research initiative (*Forschergruppe*) *Nondestructive evaluation of concrete structures using acoustic and electro-magnetic echo-method* [15] is gratefully acknowledged.

References

1. Krause, M., Mielentz, F., Milmann, B., Streicher, D., Müller, W.: Ultrasonic imaging of concrete elements: State of the art using 2D synthetic aperture. In: International Symposium of Nondestructive Testing in Civil Engineering (NDT-CE) in Berlin, Germany, 16–19 September 2003. Proceedings on BB 85-CD, V51. DGZfP, Berlin (2003)
2. Schickert, M., Krause, M., Müller, W.: Ultrasonic imaging of concrete elements using SAFT reconstruction. J. Mater. Civ. Eng. **15**(3), 235–246 (2003)
3. Mayer, K., Marklein, R., Langenberg, K.J., Kreutter, T.: Three-dimensional imaging system based on the Fourier transform synthetic aperture technique. Ultrasonics **28**, 241 (1990)
4. Langenberg, K.-J., Mayer, K., Marklein, R.: Nondestructive testing of concrete with electromagnetic and elastic waves: Modeling and imaging. Cem. Concr. Compos. **28**, 370 (2006)
5. Langenberg, K.-J., Brandfaß, M., Hannemann, R., Hofmann, C., Kaczorowski, T., Kostka, J., Marklein, R., Mayer, K., Pitsch, A.:

Inverse scattering with acoustic, electromagnetic and elastic waves as applied in nondestructive evaluation. In: Wirgin, A. (ed.) Wavefield Inversion. Springer, Vienna (1999)
6. Patentanmeldung DE 10 2006 027 132.7: Verfahren zum Detektieren von Fehlstellen in Betonbauteilen
7. Mayer, K., Langenberg, K.-J., Krause, M., Maierhofer, C., Milmann, B.: Characterization of ultrasonic and radar reflector types in concrete by phase evaluation of the signal and the reconstructed image. In: Proceedings of the ECNDT 9th European Conference on NDT, Berlin 25–29 Sept. 2006, BB 103-CD
8. Marklein, R.: EFIT simulations for Ultrasonic NDE. Proceedings of the ECNDT 2002 Conference, Barcelona, Spain, 17–21 June 2002
9. Marklein, R.: The finite integration technique as a general tool to compute acoustic, electromagnetic, elastodynamic, and coupled wave fields. In: Stone, W.R. (ed.) Review of Radio Science 1999–2002. IEEE Press, New York (2002)
10. Krause, M., Milmann, B., Schickert, M., Mayer, K.: Investigation of tendon ducts by means of ultrasonic echo methods: a comparative study. In: Proceedings of the 9th European Conference on NDT, 25–29 September 2006. BB 103-CD, Tu.3.2.1. DGZfP, Berlin (2006)
11. Streicher, D., Algernon, D., Wöstmann, J., Behrens, M., Wiggenhauser, H.: Automated NDE of post-tensioned concrete bridges using imaging echo methods. In: Proceedings of the 9th European Conference on NDT, 25–29 September 2006. BB 103-CD, We.1.3.1. DGZfP, Berlin (2006)
12. Maierhofer, C.: Nondestructive evaluation of concrete infrastructure with ground penetrating radar. J. Mater. Civ. Eng. **15**(3), 287–297 (2003)
13. Krause, M., Milmann, B., Mielentz, F., Streicher, D., Redmer, D., Mayer, K., Langenberg, K.-J.: Ultrasonic imaging methods for investigation of post-tensioned concrete structures: a study of interfaces at artificial grouting faults and its verification. This issue
14. Krause, M., Mielentz, F., Milmann, B., Streicher, D., Mayer, K.: Ultrasonic reflection properties at interfaces between concrete, steel and air: imaging and modelling. In: Al-Quadi, I., Washer, G. (eds.) Proceedings of the NDE Conference on Civil Engineering, 14–18 August 2006, St. Louis, MO, USA, pp. 472–479
15. Reinhardt, H.-W., Grosse, C.: Improvement and application of NDT methods in civil engineering in the frame of a collaborative research project funded by the German research society. In: Proceedings of the International Symposium Non-Destructive Testing in Civil Engineering (NDT-CE), 16–19 September 2003. BB 85-CD, V03. DGZfP, Berlin (2003)